Supporting Information

One Step Electrochemical Fabrication of High Performance Ni@Fe-Doped Ni(Oxy)Hydroxide Anode for Practical Alkaline Water Electrolysis

Tao Jiang[1, 5, *], Xinge Jiang[2], Jaromír Hnát[3], Alena Michalcova[4], Indro Biswas[1], Regine Reisser[1], Vasileios Kyriakou[5], Fatemeh Razmjooei[1], Hanlin Liao[2], Karel Bouzek[3], Syed-asif Ansar[1]

[1] *Institute of Technical Thermodynamics, German Aerospace Center (DLR), Stuttgart 70569, Germany*

[2] *UBFC, ICB-PMDM-LERMPS UMR6303, Sevenans 90010, France*

[3] *Department of Inorganic Technology, University of Chemistry and Technology Prague, 166 28 Prague 6, Czech Republic*

[4] *Department of Metals and Corrosion Engineering, University of Chemistry and Technology Prague, 166 28 Prague 6, Czech Republic*

[5] *Energy Systems & Conversions, Engineering and Technology Institute Groningen (ENTEG), University of Groningen, Nijenborgh 4, 9747 AG, Groningen, The Netherlands*

AUTHOR INFORMATION

Correspondence

Dr. T. Jiang: taojiang0510@gmail.com

Experimental section

Materials and chemicals

Nickel mesh (99.99 %, Pingding City Lushan Yaxing Carbon Material Co., Ltd., China); H_2SO_4 solution (99.9%, Sigma-Aldrich®); NH_4F (≥ 98.0%, Sigma-Aldrich®); $Fe(NO_3)_3 \cdot 9H_2O$ (≥ 98.0%, Sigma-Aldrich®); Ethylene glycol (≥ 99%, Sigma-Aldrich®); $Ni(NO_3)_2 \cdot 6H_2O$ (≥ 98.5%, Sigma-Aldrich®); Iridium(IV) oxide (99.9% trace metals basis, Sigma-Aldrich®).

Fabrication of CS Ni@Fe-Ni(Oxy)Hydroxide

The CS Ni@Fe-Ni(Oxy)Hydroxide was fabricated by a one-step oxidation electrodeposition (OSOE) process. Commercial perforated nickel mesh (NM, 3×2×0.3mm, effective area: 69%) was employed as soluble anode and cathode (substrate for catalysts growth). The substrate was first chemically degreased, rinsed with distilled water, and then scrubbed with alcohol and acetone. The substrate was sonicated in 1 M H_2SO_4 solution for 20 min to remove the NiO_x surface layer, rinsed with distilled water and acetone, then allowed to dry in air. After that, it was placed vertically in the electrodeposition cell of 0.35 dm^3 with magnetic stirring, parallel to the anode, with an anode-cathode distance of 5 cm. The electrodeposition cell was placed in a water bath at a suitable temperature. The OSOE process was carried out in the simplest two-electrode system. The CS Ni@Fe-Ni(Oxy)Hydroxides were in situ generated onto the cathode NM via the OSOE method by applying a certain voltage and time. The electrolyte for OSOE was an ethylene glycol-based anodizing solution (150 mL), containing 0.1 M NH_4F, 1 M deionized water, and 0.02 M $Fe(NO_3)_3$. It's worth noting that the Ni (II) was provided from the soluble anode (NM). Typically, CS Ni@ Fe-Ni(oxy)hydroxide-23 would be obtained by applying a voltage of 20 V. After 30 min's reaction, CS Ni@Fe-Ni(Oxy)Hydroxides-23 could be deposited onto the NM. After 30 min's reaction, CS Ni@Fe-Ni(Oxy)Hydroxides-23 could be deposited onto the NM. Finally, the CS Ni@Fe-Ni(Oxy)Hydroxide samples were washed three times with deionized water and ethanol and then dried in air for 15 min. The average mass loading of the as-obtained CS Ni@Fe-Ni(Oxy)Hydroxides was about 0.1 mg cm^{-2}. In the same way, CS Ni@Fe-Ni(Oxy)Hydroxide-13 (10 V, 30 min) and CS Ni@Fe-Ni(Oxy)Hydroxide-43 (40 V, 30 min) were prepared with average mass loading of 0.075 and 0.15 mg cm^{-2}, respectively.

Fabrication of CS Ni@Ni(Oxy)Hydroxide

The preparation process of bare CS Ni@Ni(Oxy)Hydroxide-23 was similar to that of CS Ni@Fe-Ni(Oxy)Hydroxide-23, except for the precursor recipe. For CS Ni@Ni(Oxy)Hydroxide-23, 0.02 M $Fe(NO_3)_3$ was changed to 0.02 M $Ni(NO_3)_2$. The other solutions and processes were the same as the fabrication of CS Ni@Ni(Oxy)Hydroxide-23. The average mass loading of the as-obtained CS Ni@Ni(Oxy)Hydroxide nanoarray was about 0.15 mg cm^{-2}.

Fabrication of IrO_2/NM electrode

To prepare the IrO_2/NM electrodes, 40 mg IrO_2, 60 μL Nafion, 540 μL ethanol, and 400 μL deionized water were ultrasonicated for 60 min to obtain a homogeneous dispersion. Then, a piece of clean NM was dipped into the dispersion, which was then dried in air at 60 °C for 4 h. The mass loading of the IrO_2 catalyst on NM was controlled to be ~ 0.1 mg cm^{-2}, just close to that of Ni@Fe-Ni(Oxy)Hydroxide-23.

Materials characterization

XRD was performed with Bruker AXS D8 focus, equipped with a cobalt anticathode (λ =

1.78897 Å), and operated at 35 kV, 40 mA. SEM was carried out using a JEOL-JSM-7800F system equipped with an EDS analysis system (BRUCKER SDDX-Flash 6130; Zeiss Gemini Ultra plus microscope). The contact angle measurement was carried out by dropping 6 μL deionized water on the electrode surface with a dosing rate of 1 μL s−1 (DataPhysics Optical Contact Angle System OCA 15EC) and the data were analyzed with the SCA20 software. The measurements were conducted more than 3 times per sample to increase the accuracy of the data. UHV-XPS analysis has been performed using a Thermo Scientific ESCALAB 250 ultra-high vacuum (UHV) facility operated at a pressure of 1×10^{-9} mbar. As an X-ray source (Thermo XR4) the Al Kα line was used. The detection spot at the sample was covering an area of 0.8 mm^2. The depth profiles were determined by high energy Ar^+-sputtering using a Thermo EX05 ion gun at the flowing sputtering conditions: $2-3\times10^{-8}$ mbar at partial pressure, 3−7 μA Ar^+ current at a sample area of 3×4 mm^2, 2 kV acceleration voltage, and 10 mA emission current. Transmission electron microscopy (TEM) bright-field imaging, high-resolution TEM, selected area electron diffraction (SAED), high-angle annular dark-field scanning TEM (HAADF-STEM), and electron energy-loss spectroscopy (EELS) mapping are performed on a field-emission analytical electron microscope (FEI Tecnai G2 F20 X-TWIN) operating at 200 kV. The camera length was 87 mm. The collection angle was 29, 36 mrad. The energy resolution was 0.7 eV. Distilled water and ethanol were used to thoroughly clean all the samples before testing commenced.

Electrochemical half-cell measurements (three-electrode test benches)

All electrochemical measurements were carried out using a ZAHNER ZENNIUM X boosted by PP241 Electrochemical Workstation with a developed in-house three-electrode test bench. Hydrogen Reference Electrode HydroFlex (Gaskatel GmbH, Germany) was used as the reference electrode. The potential measured using this Hydrogen Reference Electrode (HRE) as the reference electrode didn't require any complex conversion to Reversible Hydrogen Electrode (RHE), allowing any tested temperature and pH of the electrolyte, namely $E_{RHE} = E_{HRE}$. Furthermore, HRE is suitable for the full pH range from −2 to 16 and temperature range from −30 °C to 200 °C. Even if we tested at temperatures above room temperature (25 °C) and high concentrations (30 wt.% KOH), the data remained stable and reliable. Pt foil (10 mm×10 mm×0.2 mm, in 1 M KOH measurement) and bare nickel mesh (Φ 32 mm, in 30 wt.% KOH measurement) were used as the counter electrode (CE). The bare NM, NM/CS Ni@Ni(Oxy)Hydroxide sample, and NM/CS Ni@Fe-Ni(Oxy)Hydroxide samples were used directly as the working electrode, without further treatments. All the samples' geometric size is 10 mm×10 mm (1×0.69 cm^2 effective area) in 1 M KOH measurement and Φ 30 mm (homemade electrode clips ensure an effective area of 4×0.69 cm^2) in 30 wt.% KOH measurement. To better illustrate the catalytic activity of the materials, we tested all the samples under 1 M KOH at room temperature. In addition, for the target NM/CS Ni@Fe-Ni(Oxy)Hydroxide-23 sample, 30 wt.% KOH at 70 °C (which refers to industrial applications) was employed to run a 500 h long-term stability test (circular bare NM with 4×0.69 cm^2 effective area as the counter electrode). The current density values of LSV curves in this study refer to the geometric surface area. 1 M KOH solutions were saturated with O_2 before OER tests at room temperature.

The overpotential (η) was calculated by using the formula: $\eta\ (V) = E_{RHE} - 1.229$ V. Linear sweep voltammogram (LSV) curves were recorded at a scan rate of 5 mV s^{-1}, and each

measurement was repeated at least three times to avoid any incidental error. Tafel slopes were derived from OER LSV obtained by plotting overpotential against log (j, current density) after iR correction ($E_{iR}=E-j\times R_s$) in all the above test conditions. The electrochemical impedance spectroscopy (EIS) measurement was conducted in the frequency range of 100 kHz to 0.1 Hz with an amplitude of 5 mV under a fixed bias of 1.53 V vs. RHE (η = 300 mV).

The ECSA was determined by measuring the capacitive current associated with double-layer charging from the scan-rate dependence of CVs. For this, the potential window of CVs was 1.07 – 1.17 V vs. RHE. The scan rates were 5, 10,20, 40, 60,80 and 100 mV s^{-1}. The double-layer capacitance (C_{dl}) was estimated by plotting the $\Delta J = (J_a - J_C)$ at 1.12 V vs. RHE against the scan rate. The linear slope is twice the double-layer capacitance C_{dl}. The ECSA values were calculated from the measured double-layer capacitance divided by the specific capacitance of an atomically smooth material ($C_{dl'}$, ~40 μF cm^{-2}): ECSA = C_{dl} / $C_{dl'}$ × S, where S is the actual surface area of the electrode.[1]

The turnover frequency (TOF) is a very important kinetic parameter for OER. TOF shows the intrinsic property of the catalysts, which is important for evaluating the performance of the catalysts. The TOF value was calculated from the equation: TOF = (j × A) / (4 × n × F), where j is the current density at an overpotential of 300 mV for OER, A is the geometric surface area of the NM electrode, F is the Faraday constant (96485 C mol^{-1}), and n is the mole number of the active catalysts (Ni(Oxy)Hydroxide/IrO_2) on the electrode calculated by the loading and the S/TEM (EELS) spectra analyses. All the Ni/Fe atoms in the Ni(Oxy)Hydroxide of CS Ni@Ni(Oxy)Hydroxide sample and CS Ni@Fe-Ni(Oxy)Hydroxide samples were assumed to be accessible for catalyzing water splitting.

e.g. Ni@Fe-Ni(Oxy)Hydroxide: (the main composition is $(Ni(OH)_2(NiOOH)_{0.167})_{0.857}$, which can be confirmed by TEM and XRD analysis: Crystal structure of the Ni@Fe-Ni(Oxy)Hydroxide matched well with that of JCPDS 89-7111($(Ni(OH)_2(NiOOH)_{0.167})_{0.857}$) from the XRD analysis; especially, the lattice fringes (HR-TEM: Figure 1f) with distances of 0.242 nm and 0.227 nm (included angle: ≈125°), were very consistent with (104) and (015) planes of JCPDS 89-7111($(Ni(OH)_2(NiOOH)_{0.167})_{0.857}$)).

$M_{Ni@Fe\text{-}Ni(Oxy)Hydroxide}$ (4.1 at. % Fe doping; from EELS analysis) ≈ $M_{(Ni(OH)2(NiOOH)0.167)0.857)}$ = 92.57 g mol^{-1};

n = m/M = 0.1 mg/92.57 g mol^{-1};

$j_{300\ mV}$ = 118.8 mA cm^{-2} (from Figure 3a);

$TOF_{(Ni@Fe\text{-}Ni(Oxy)Hydroxide)}$

= (j × A) / (4 × n × F)

= (118.8 mA cm^{-2}×1 cm^2)/(4×(0.1×10^{-4} g/92.57 g mol^{-1})×96485 C mol^{-1}) = 0.285 s^{-1}.

Chronopotentiometry measurements were performed to evaluate the long-term stability. The oxygen and hydrogen were collected using the water displacement method during the water splitting electrolyzer test (CS Ni@Ni(Oxy)Hydroxide-23 as both anode and cathode), and then the Faradaic Efficiency was calculated for both OER and HER.

The evolved oxygen and hydrogen gas on the electrode were separately collected with a 10 mL graduated cylinder, which was filled with electrolyte. Constant-current electrolysis was carried out at a current density of 50 mA cm^{-2} under standard conditions (25 °C, 1 atm) for a total of 24 min. During the test, we recorded the volume of collected oxygen and hydrogen gas every 3 min. The accumulated charge passing through the working electrode was calculated by the

equation: Q=It, where I is the electrolysis current and t is the electrolysis time. Therefore, the Faradaic efficiency can be calculated as follows,

$FE_{O2} = (4 \times 96485 \times n_{O2}) / (Q_{OER})$

$n_{O2} = V_{O2} / V_m$

$FE_{H2} = (2 \times 96485 \times n_{H2}) / (Q_{HER})$

$N_{H2} = V_{H2} / V_m$

$Q = I \times t$

where the n is the amount of evolved gas, V is the volume of evolved gas obtained by the water displacement method, V_m is molar volume 22.4 L mol^{-1}, I is the electrolysis current and t is the electrolysis time, and Q is the total charge passed through electrode (Figure S13).

AEL cell measurements (4 cm^2, full cell test)

A homemade AEL cell (active surface area of 4 cm^2) driven by Autolab PGSTAT128N (equipped with a 10A booster) was employed to examine the performance of the prepared anodes. Square-shaped 4 cm^2 CS Ni@Fe-Ni(Oxy)Hydroxide-23 as the anode and bare Ni mesh (NM) as the cathode was assembled horizontally with Zirfon PERL (500 μm) supplied by Agfa as a separator in the configuration using two Ni bipolar plates as current collectors, which were reinforced with four bolts. Nickel foams were used as gas diffusion layers (GDLs) on both sides of the AEL cell. The cells were operated vertically, and 6 M KOH electrolytes were surrounded on two separate sides. Heating was performed by an electromagnetic stirrer, and the temperature was increased to 70 °C before starting the cell. After 30 min of activation at a constant current density of 0.3 A cm^{-2}, the cells were characterized by recording I-V curves with a scan rate of 10 mV/s and the max current up to 8 A. As a reference, one cell with bare NM at both the anode and cathode sides with Zirfon as a separator is also tested in the same condition. Electrochemical Impedance Spectroscopy (EIS) was performed in galvanostatic mode with the workstation Autolab PGSTAT128N (equipped 10A booster) in a frequency range from 100 mHz to 50 kHz. To analyze the EIS plots, the fitting procedure was performed using the equivalent circuit chosen based on the physical processes and their interactions in the system, which include ohmic, cathodic charge transfer (HER), anodic charge transfer (OER), and mass-transfer resistances. The fitting of the Nyquist plot is done by the commercially available ZView®.[2]

Table S1. EELS element contents of CS Ni@Fe-Ni(Oxy)Hydroxide-23 and CS Ni@Ni(Oxy)Hydroxide-23.

Samples	**Ni/at.%**	**Fe/at.%**	**O/at.%**
CS Ni@Fe-Ni(Oxy)Hydroxide-23	52 ± 3	4.1 ± 0.2	44 ± 2
CS Ni@Ni(Oxy)Hydroxide-23	51 ± 3	0	48 ± 3

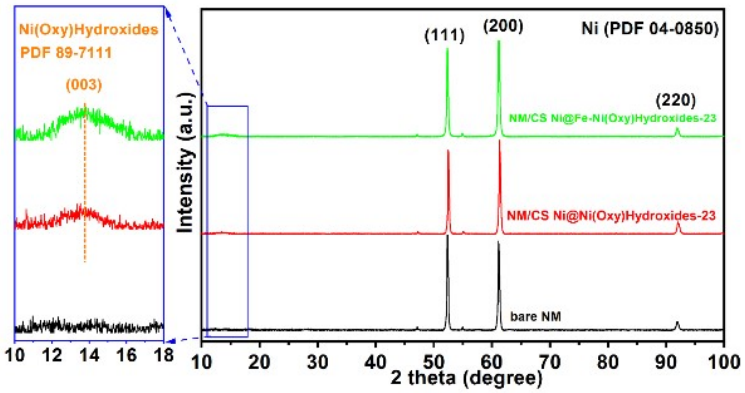

Figure S1. XRD patterns of the bare NM, NM/CS Ni@Ni(Oxy)Hydroxide-23, and NM/CS Ni@Fe-Ni(Oxy)Hydroxide-23. "All the XRD data was tested with the Cobalt target. Note: small reflections at 2θ of ~47° and ~55° may be caused by the employed Cobalt target.

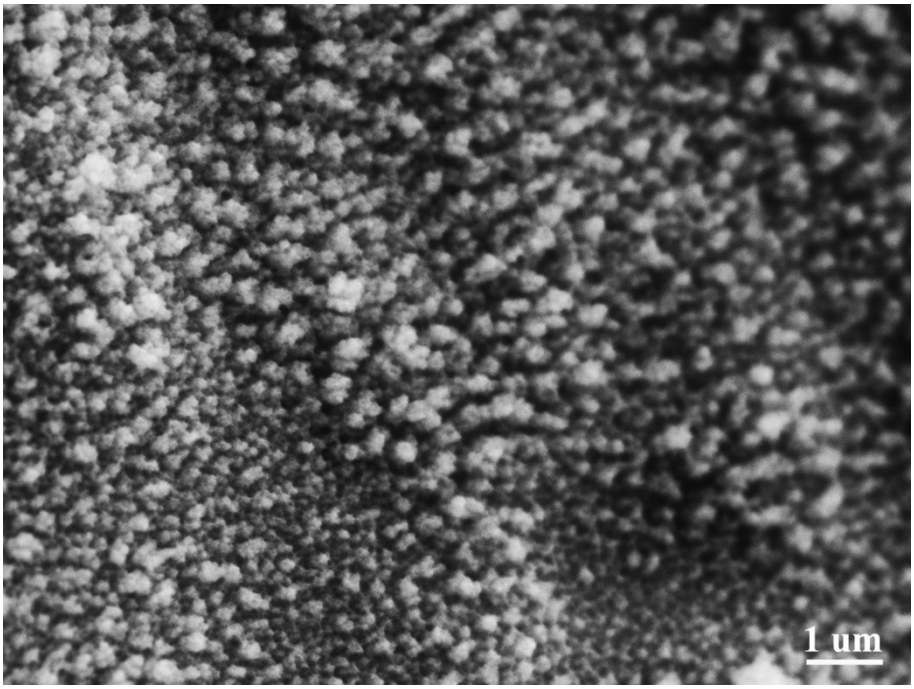

Figure S2. Low-magnification SEM image of the top surface of CS Ni@Fe-Ni(Oxy)Hydroxide-23.

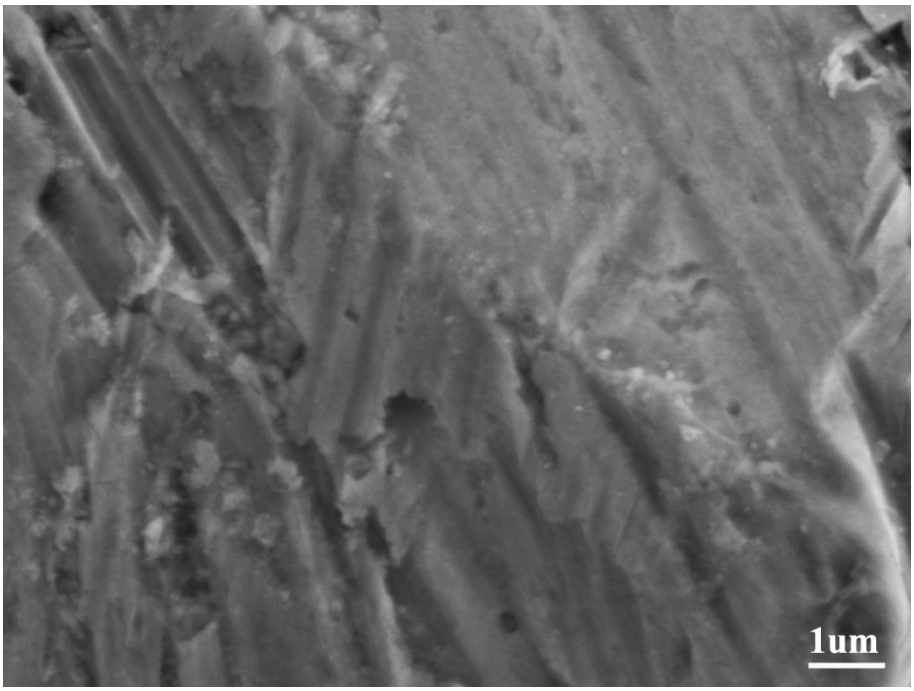

Figure S3. SEM image of the top surface of NM substrate.

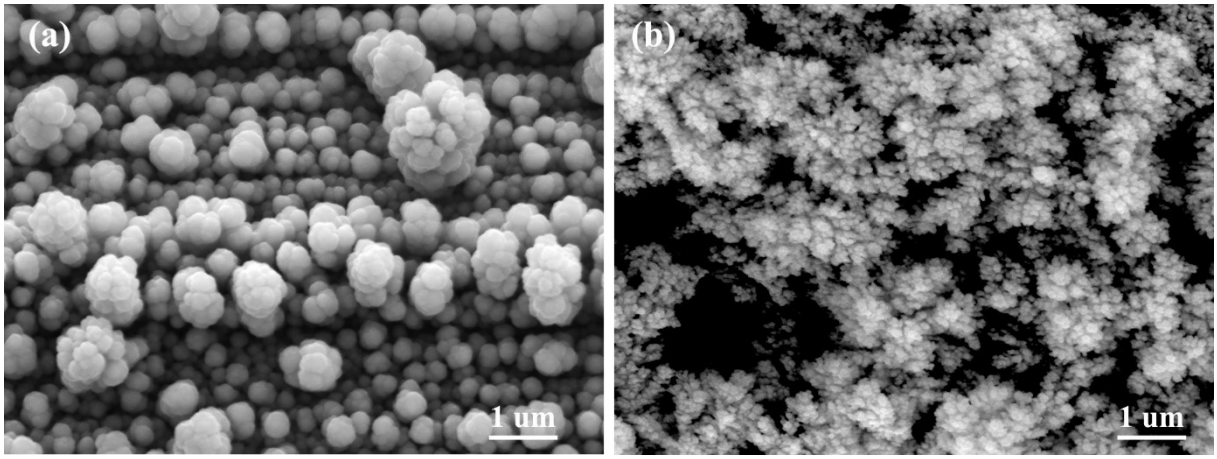

Figure S4. SEM images of the top surface of Ni@Fe-Ni(Oxy)Hydroxide samples. (a) Ni@Fe-Ni(Oxy)Hydroxide-13; (b) Ni@Fe-Ni(Oxy)Hydroxide-43.

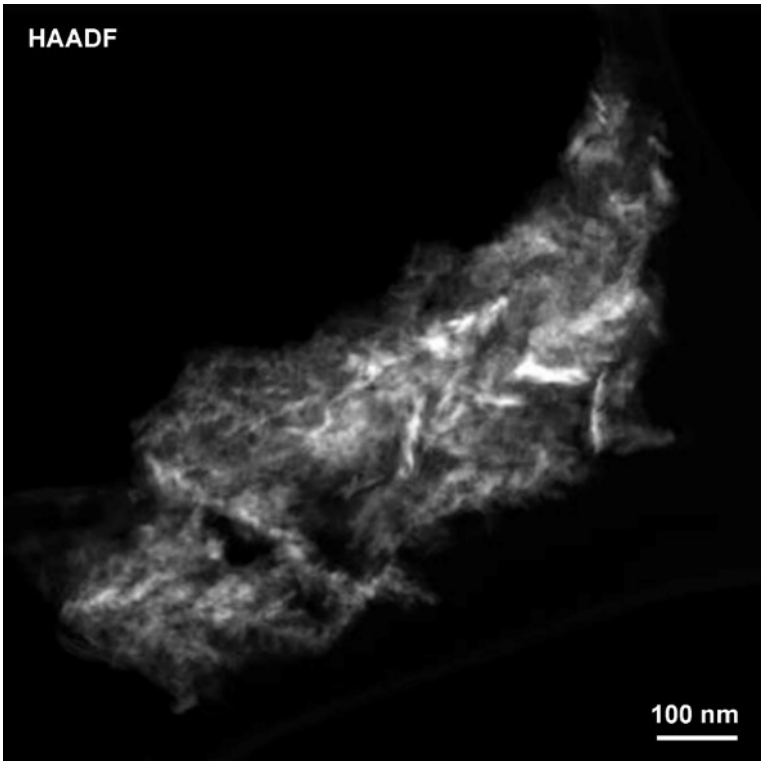

Figure S5. HAADF image of the CS Ni@Fe-Ni(Oxy)Hydroxide-23 nanoarray.

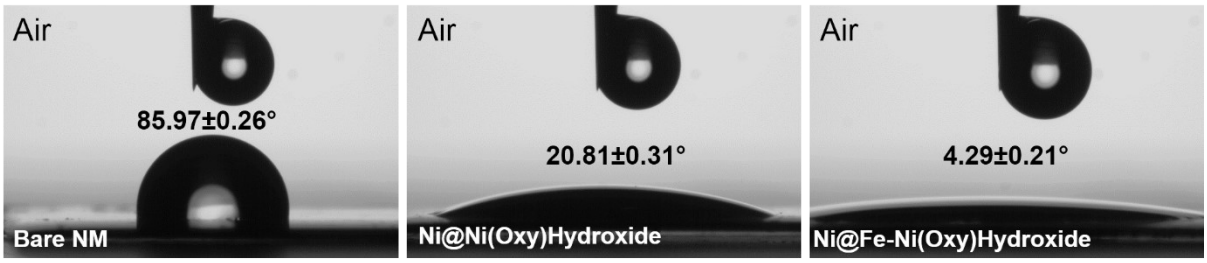

Figure S6. The hydrophilicity of the samples.

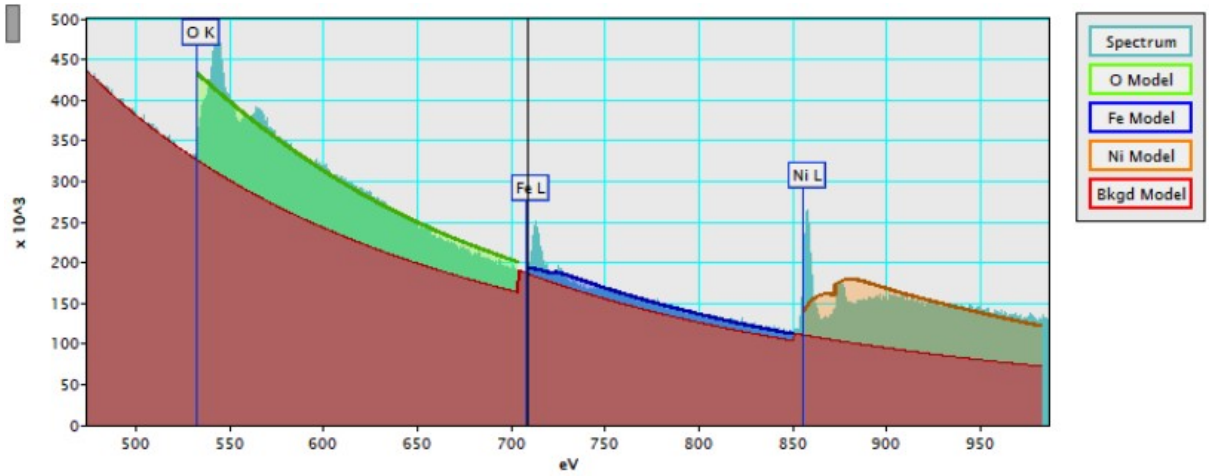

Figure S7. EELS spectra of the O-K edge, Fe-$L_{2,3}$ edges, and Ni-$L_{2,3}$ edges from the CS Ni@Fe-Ni(Oxy)Hydroxide-23.

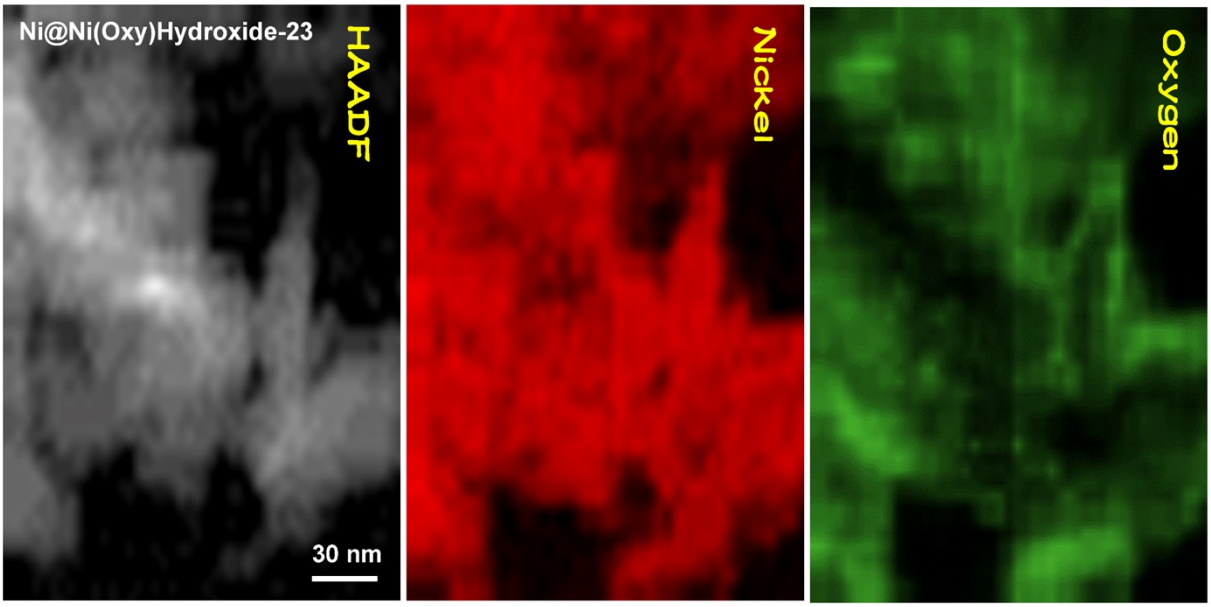

Figure S8. EELS elemental mapping images of the CS Ni@Ni(Oxy)Hydroxide-23 sample.

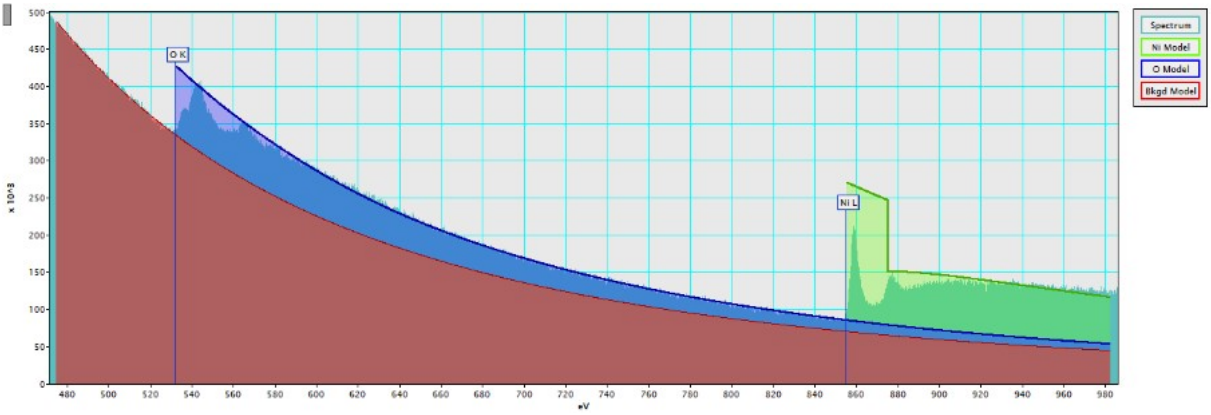

Figure S9. EELS spectra of the O-K edge, and Ni-$L_{2,3}$ edges from the CS Ni@Ni(Oxy)Hydroxide-23.

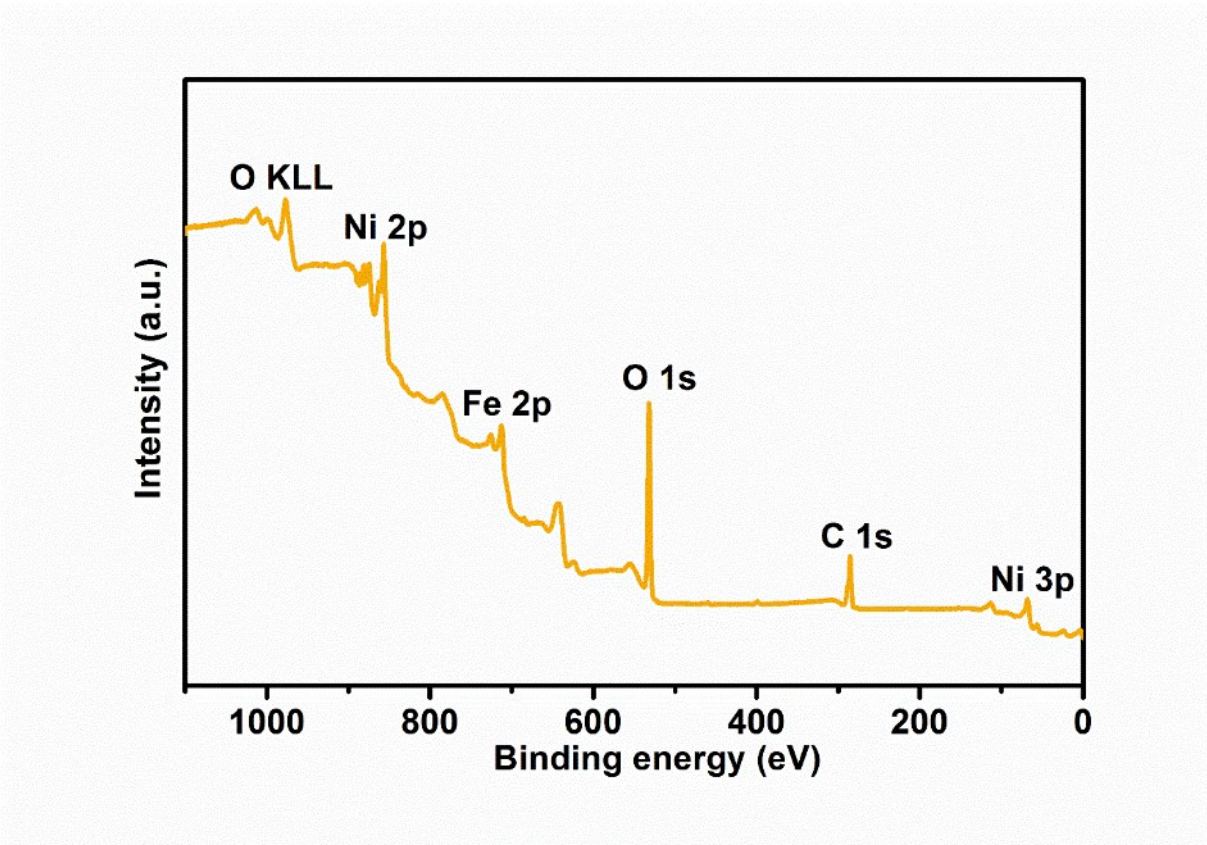

Figure S10. The wide scanning XPS spectrum of the CS Ni@Fe-Ni(oxy)hydroxide-23 sample.

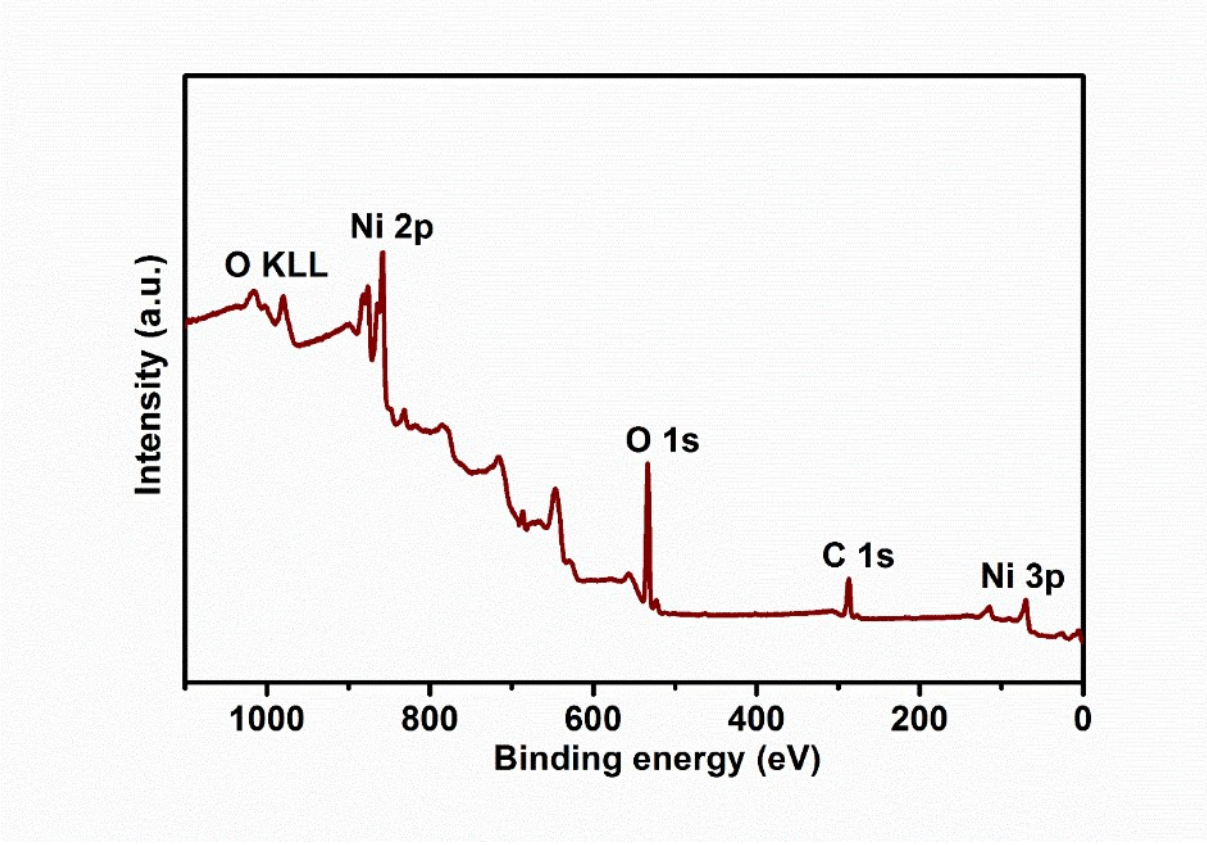

Figure S11. The wide scanning XPS spectrum of the CS Ni@Ni(oxy)hydroxide-23 sample.

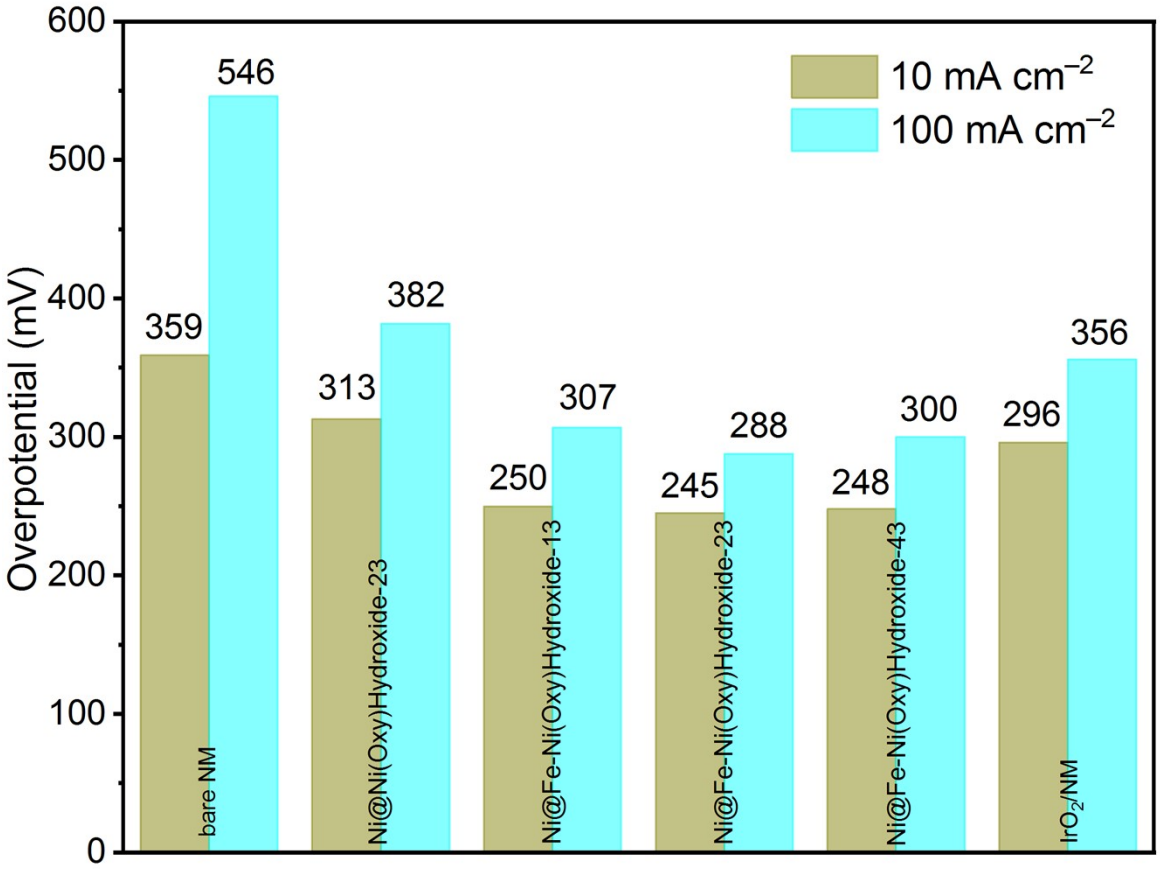

Figure S12. Overpotentials at the geometric current density of 10 mA cm^{-2} and 100 mA cm^{-2} were illustrated and compared.

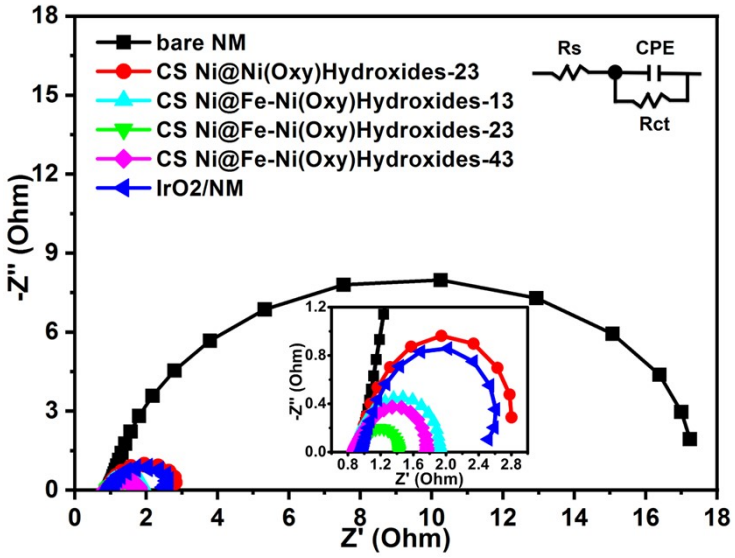

Figure S13. Electrochemical impedance spectroscopy (EIS) data of the Ni(Oxy)Hydroxide samples and the control samples.

Table S2. The simulated equivalent circuit data of the employing samples.

Samples	R_s / Ω cm^2	R_{ct} / Ω cm^2	CPE-T/S•s^(CPE-P)•cm^(–2)	CPE-P
IrO_2/NM	0.87	1.76	5.52×10^{-2}	0.86
CS Ni@Fe-Ni(Oxy)Hydroxide-13	0.85	1.08	1.11×10^{-2}	0.89
CS Ni@Fe-Ni(Oxy)Hydroxide-23	0.85	0.58	3.10×10^{-2}	0.86
CS Ni@Fe-Ni(Oxy)Hydroxide-43	0.87	0.89	5.03×10^{-2}	0.91
CS Ni@Ni(Oxy)Hydroxide-23	0.85	1.99	9.43×10^{-2}	0.92
bare NM	0.95	17.66	3.90×10^{-3}	0.91

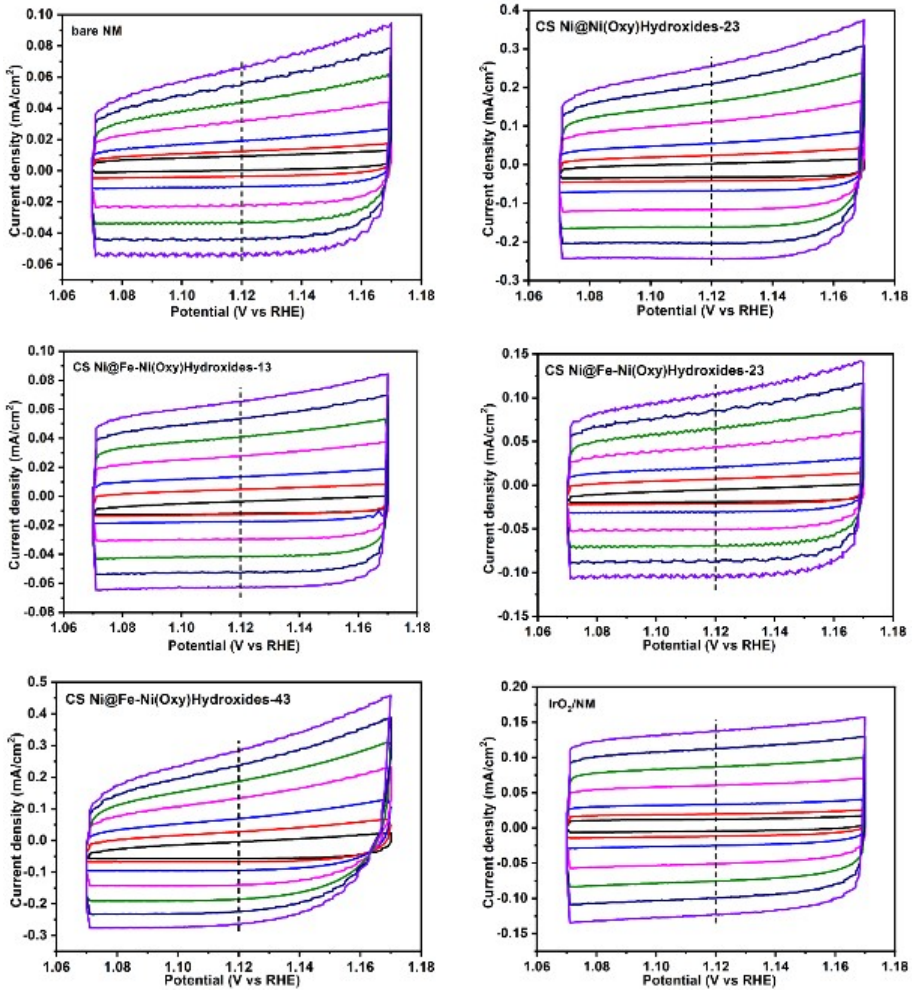

Figure S14. CV curves at different scan rates. the potential window of CVs was 1.07 – 1.17 V vs. RHE. The scan rates were 5, 10,20, 40, 60,80 and 100 mV s^{-1}. The double-layer capacitance (Cdl) was estimated by plotting the $\Delta J = (Ja - JC)$ at 1.12 V vs. RHE against the scan rate.

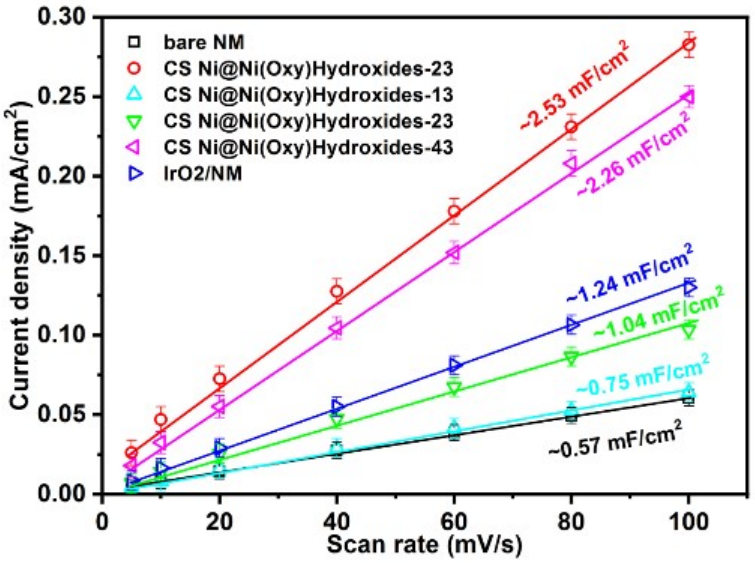

Figure S15. The corresponding C_{dl} of all the samples. The double-layer capacitance (C_{dl}) was estimated by plotting the $\Delta J = (J_a - J_C)$ at 1.12 V vs. RHE against the scan rate. The linear slope is twice the double-layer capacitance C_{dl}.

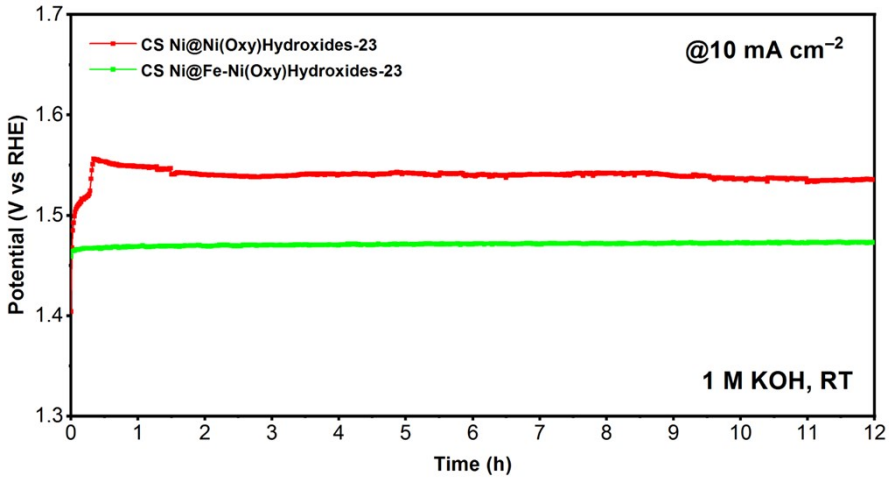

Figure S16. Chronoamperometric measurements at 10 mA cm^{-2} of CS Ni@Ni(Oxy)Hydroxide-23 sample and CS Ni@Fe-Ni(Oxy)Hydroxide-23 sample.

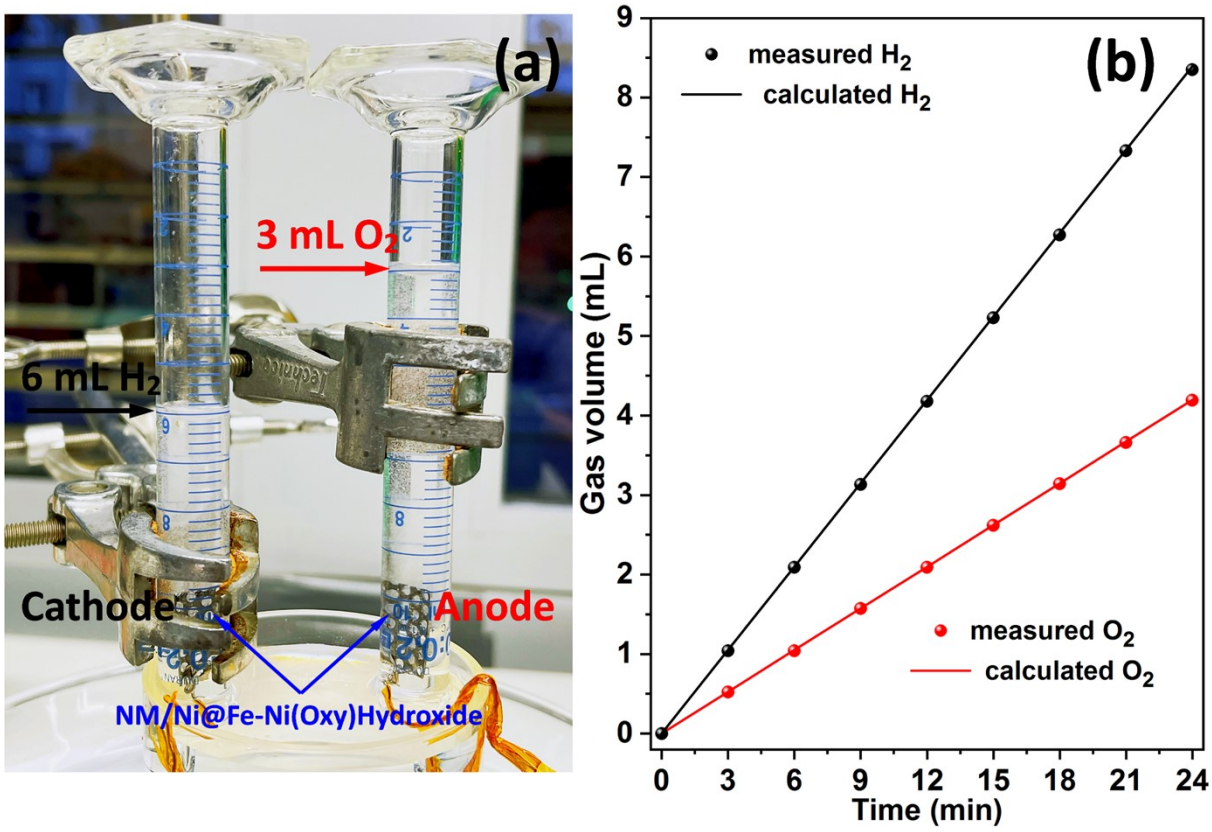

Figure S17. (a) Digital photograph of H_2 and O_2 gas evolution on CS Ni@Ni(Oxy)Hydroxide-23 using the water displacement method. (b) Experimental and theoretical amounts of H_2 and O_2 generated by CS Ni@Ni(Oxy)Hydroxide-23 electrodes at a fixed current density of 50 mA cm^{-2}.

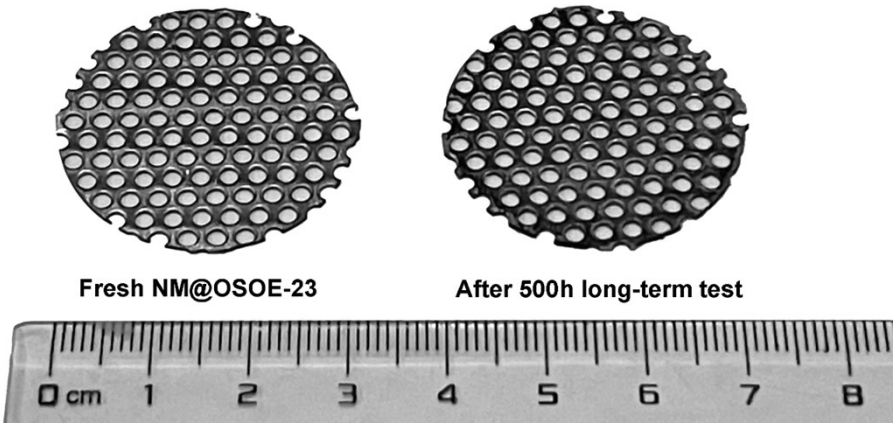

Figure S18. Photos of the CS Ni@Fe-Ni(Oxy)Hydroxide-23 electrode after durability test with 500 hours at 500 mA cm^{-2}.

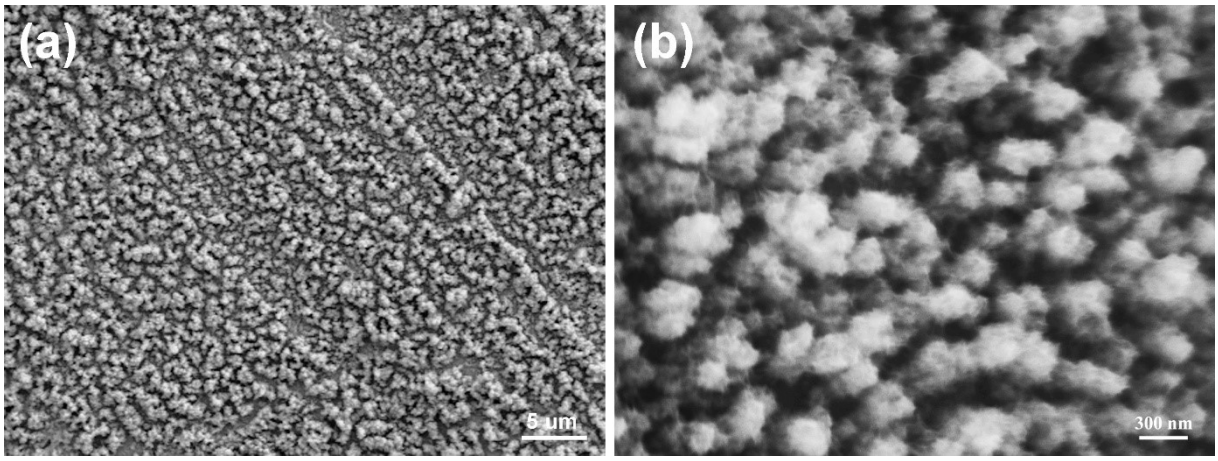

Figure S19. SEM images of the CS Ni@Fe-Ni(Oxy)Hydroxide-23 electrode after durability test with 500 hours at 500 mA cm^{-2}.

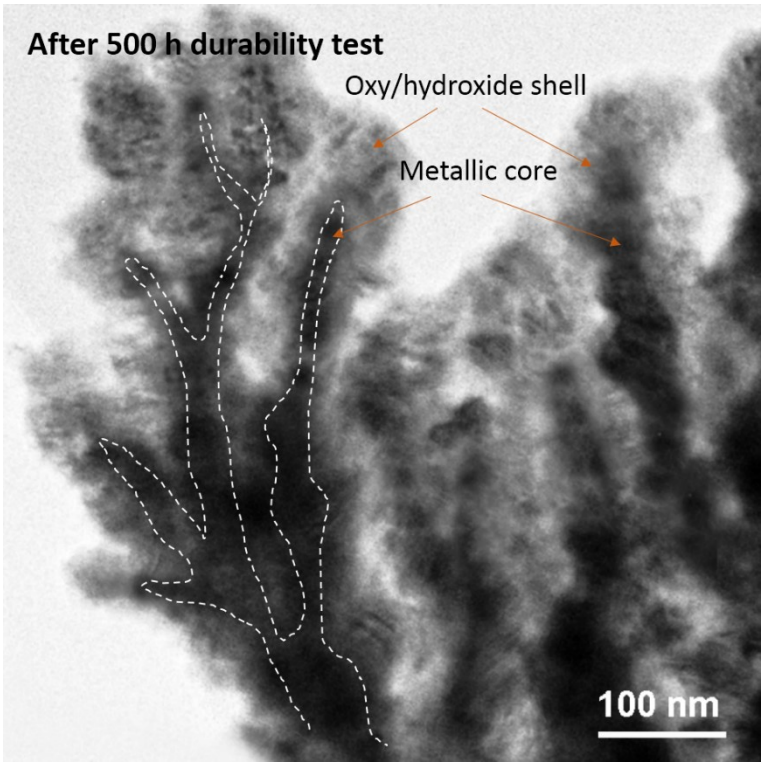

Figure S20. TEM image of the CS Ni@Fe-Ni(Oxy)Hydroxide-23 electrode after durability test with 500 hours at 500 mA cm^{-2}.

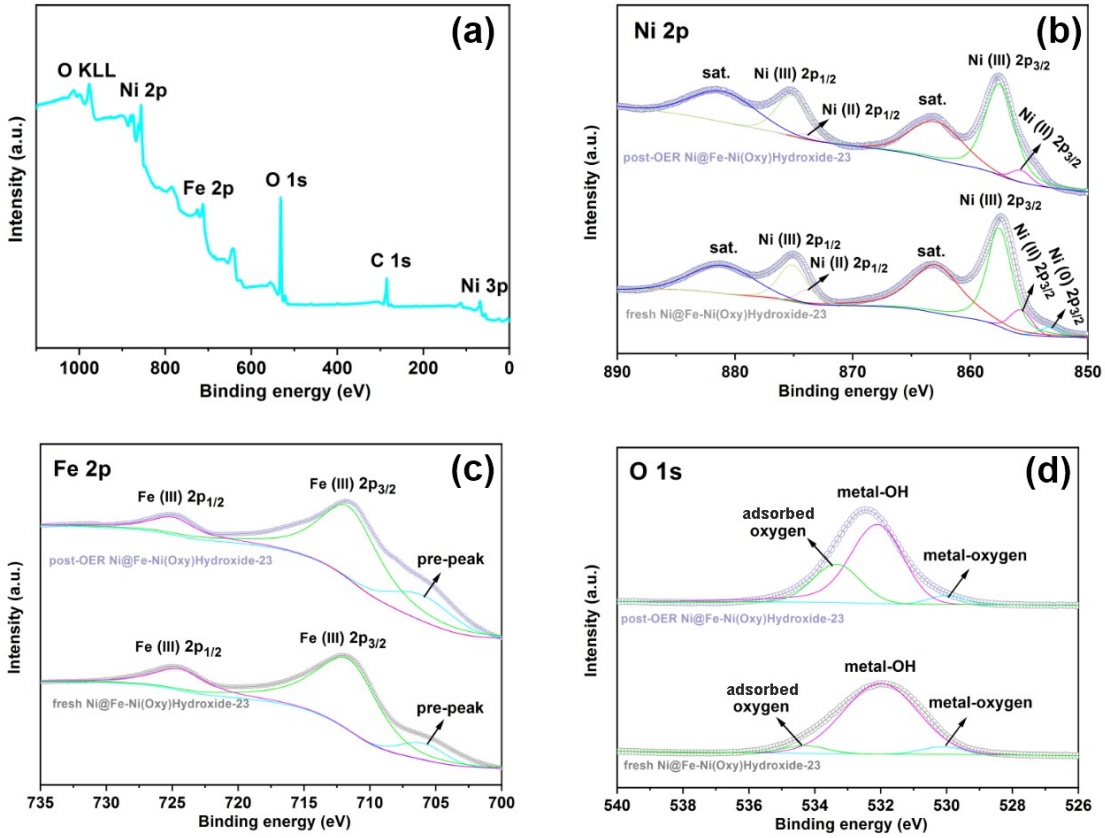

Figure S21. The survey scan and high-resolution XPS spectra of the post-OER CS Ni@Fe-Ni(Oxy)Hydroxide-23. (a) survey scan, (b) Ni 2p, (c) Fe 2p, (c) O 1s.

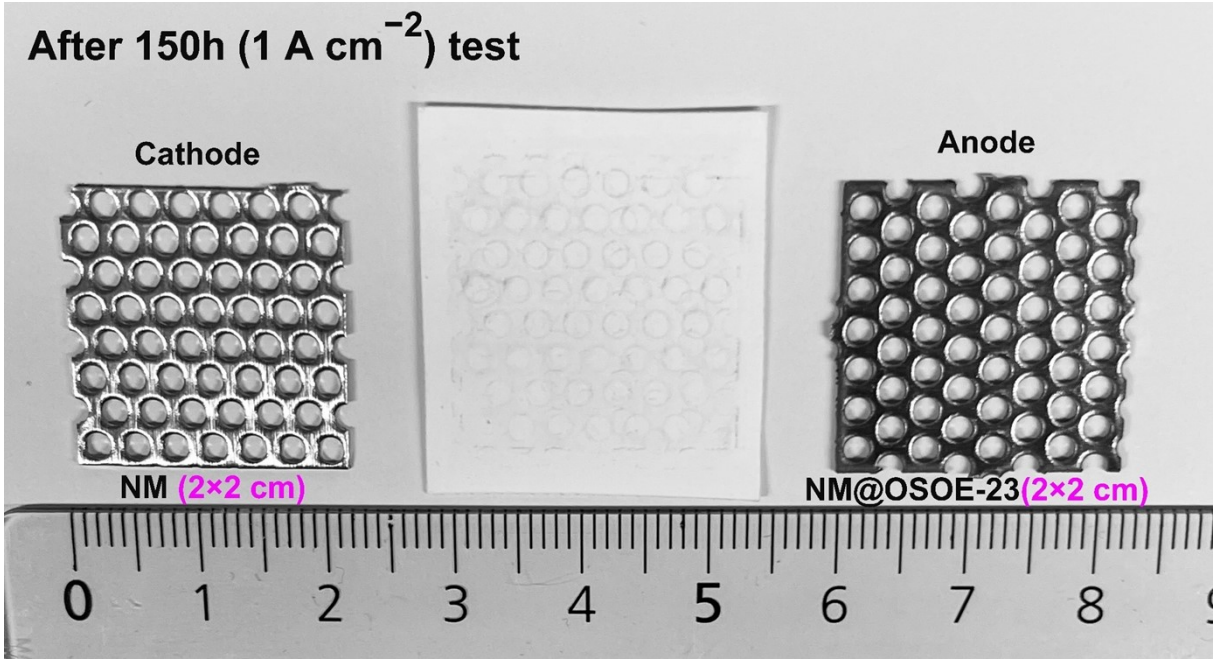

Figure S22. The photo of the 4 cm^2 squared NM@OSOE-23 electrode after 150 h test with 1A cm^{-2}.

Table S3. The OER activity of the prepared catalysts compared with state-of-the-art OER catalysts reported.

Materials	**Loading, mg cm^{-2}**	**Electrolyte**	**η (mA cm^{-2}), mV**		**Tafel slope, mV/dec**	**TOF, s^{-1}**	**Mass activity, A g^{-1}**	**Reference**
CS Ni@Fe-Ni(Oxy)Hydroxide	**0.1**	**1 M KOH**	**245 (η_{10})**	**288 (η_{100})**	**37**	**0.285 @300 mV**	**1336 (catalyst loading) @300 mV**	**This work**
IrO_2	**0.15**	**1 M KOH**	**269 (η_{10})**	**356 (η_{100})**	**55**	**0.036 @300 mV**	**136 (metal) @300 mV**	**This work**
ZnCo-LDH	0.32	0.1 M KOH	490* (η_{10})	N/A	61	0.0245 @300 mV	51 @500 mV	J. Mater. Chem. A, 2014 [3]
Ni-P-B	6.15	1 M KOH	263 (η_{50})	N/A	70.6	3.45 @300 mV	N/A	Energy Environ. Sci., 2019 [4]
IrO_2	6.0	1 M KOH	N/A	N/A	83	2.37 @300 mV	N/A	Energy Environ. Sci., 2019 [4]
$Ni_3Fe_{0.5}V_{0.5}$	0.27	1 M KOH	200 (η_{10})	263 (η_{100})	39	0.574@300 mV	N/A	Nat. Commun., 2018 [5].
Co-Fe-Cr (oxy)Hydroxides	0.20	1 M KOH	232 (η_{10})	N/A	31	0.230@300 mV	773.1 (metal) @300 mV	Adv. Energy Mater., 2021 [6]
OESSC	N/A	1 M KOH	290 (η_{10})	320 (η_{100})	38	0.0061@290 mV	N/A	Appl. Catal. B, 2019 [7]
ACO/Ag	0.28	1 M KOH	271 (η_{10})	N/A	N/A	0.0417@300 mV	N/A	Nano Energy, 2019 [8]
$V_{2.5}$-$CoNiSe_2$	0.4	1 M KOH	252 (η_{10})	N/A	N/A	N/A	N/A	J. Power Sources, 2021 [9]
F-$CoMoO_4$	4.26	1 M KOH	256 (η_{10})	341 (η_{100})	64	N/A	N/A	Appl. Catal. B, 2022 [10]
$Sr_3Ir_2O_7$	N/A	1 M KOH	269 (η_{10})	N/A	53	N/A	165@300 mV	Chem. Eng. J., 2021 [11]
NF/NiSe@Fe_2O_3	N/A	1 M KOH	200 (η_{10})	278 (η_{100})	37	N/A	N/A	Sci. Bull., 2021 [12]
NiFeP/MXene	N/A	1 M KOH	286 (η_{10})	N/A	35	0.35@300 mV	N/A	Sci. Bull., 2021 [13]
CoFe-MOF-OH	0.212	1 M KOH	265 (η_{10})	N/A	44	0.4004@400 mV	N/A	ACS Catalysis, 2019 [14]
NiFeMOFs	N/A	1 M KOH	258 (η_{10})	326 (η_{100})	49	1.80@350 mV	N/A	Adv. Energy Mater., 2021 [15]
Ni-MOFs	1	1 M KOH	280 (η_{50})	321 (η_{100})	49	N/A	N/A	Inorg. Chem. Front., 2022 [16]
MnSe@MWCNT	N/A	1 M KOH	290 (η_{10})	N/A	55	N/A	N/A	J. Mater. Chem. A, 2022 [17]
Fe-Co_9S_8@SNC	0.5	1 M KOH	273 (η_{10})	343 (η_{100})	56	N/A	N/A	Nano Res. 2022 [18]

*Overpotentials were estimated from the polarization curves presented in the reference literature.

References

1. C. Liang, Zou, P., Nairan, A., Zhang, Y., Liu, J., Liu, K., ... & Yang, C., *Energy Environ. Sci.*, 2020, **13**, 86-95.
2. D. J. S. A. Johnson, Inc, 2000.
3. Y. Li, Zhang, L., Xiang, X., Yan, D., & Li, F., *J. Mater. Chem. A*, 2014, **2**, 13250-13258.
4. W. Hao, R. Wu, H. Huang, X. Ou, L. Wang, D. Sun, X. Ma and Y. Guo, *Energy Environ. Sci.*, 2020, **13**, 102-110.
5. J. Jiang, Sun, F., Zhou, S., Hu, W., Zhang, H., Dong, J., ... & Wang, M., *Nat. Commun.*, 2018, **9**, 1-12.
6. J. Chen, H. Li, S. Chen, J. Fei, C. Liu, Z. Yu and Y. Chen, *Adv. Energy Mater.*, 2021, **11**, 2003412.
7. Y. Lyu, R. Wang, L. Tao, Y. Zou, H. Zhou, T. Liu, Y. Zhou, J. Huo, S. P. Jiang, J. Zheng and S. Wang, *Appl. Catal. B*, 2019, **248**, 277-285.
8. R. Zhang, Z. Sun, C. Zong, Z. Lin, H. Huang, K. Yang, J. Chen, S. Liu, M. Huang, Y. Yang, W. Zhang and Q. Chen, *Nano Energy*, 2019, **57**, 753-760.
9. A. El Jaouhari, A. Slassi, B. Zhang, A. Pershin, W. Liu, D. Cornil and J. Zhu, *J. Power Sources*, 2021, **514**, 230596.
10. W. Xie, J. Huang and Y. Wang, *Applied Catalysis B: Environmental*, 2022, **303**, 120871.
11. C. Zhu, H. Tian, B. Huang, G. Cai, C. Yuan, Y. Zhang and M. R. Li, *Chem. Eng. J.*, 2021, **423**, 130185.
12. K. Guo, Y. Wang, S. Yang, J. Huang, Z. Zou, H. Pan and C. Xu, *Science Bulletin*, 2021, **66**, 52-61.
13. J. Chen, Q. Long, K. Xiao, T. Ouyang, N. Li, S. Ye and Z. Q. Liu, *Science Bulletin*, 2021, **66**, 1063-1072.
14. Z. Zou, T. Wang, X. Zhao, W. J. Jiang, H. Pan, D. Gao and C. Xu, *ACS Catalysis*, 2019, **9**, 7356-7364.
15. Y. Wang, B. Liu, X. Shen, H. Arandiyan, T. Zhao, Y. Li and C. Zhao, *Adv. Energy Mater.*, 2021, **11**, 2003759.
16. X. Wang, X. Wang, L. Zhao, H. Zhang, M. Liu, C. Zhang and S. Liu, *Inorganic Chemistry Frontiers*, 2022, **9**, 179-185.
17. H. Singh, M. Marley-Hines, S. Chakravarty and M. Nath, *J. Mater. Chem. A*, 2022, **10**, 6772-6784.
18. W. Wang, Y. Yang, Y. Zhao, S. Wang, X. Ai, J. Fang and Y. Liu, *Nano Research*, 2022, **15**, 872-880.